

LA-UR-15-21513

Approved for public release; distribution is unlimited.

Title: In-Situ DIC and Strain Gauges to Isolate the Deficiencies in a Model for Indentation Including Anisotropic Plasticity

Author(s): Prime, Michael Bruce
Merson, Jacob Simon
Lovato, Manuel L.
Liu, Cheng

Intended for: SEM 2015 Annual Conference and Exposition on Experimental and Applied Mechanics, 2015-06-08/2015-06-11 (Costa Mesa, California, United States)

Issued: 2015-03-02

Final Reference is a book chapter in the conference proceedings series:

Merson, J. S., Prime, M. B., Lovato, M. L., and Liu, C., 2016, "In-Situ DIC and Strain Gauges to Isolate the Deficiencies in a Model for Indentation Including Anisotropic Plasticity," Residual Stress, Thermomechanics & Infrared Imaging, Hybrid Techniques and Inverse Problems, Volume 9, S. Bossuyt, G. Schajer, and A. Carpinteri, eds., Springer International Publishing, pp. 183-197.

Available at: http://dx.doi.org/10.1007/978-3-319-21765-9_24

Disclaimer:

Los Alamos National Laboratory, an affirmative action/equal opportunity employer, is operated by the Los Alamos National Security, LLC for the National Nuclear Security Administration of the U.S. Department of Energy under contract DE-AC52-06NA25396. By approving this article, the publisher recognizes that the U.S. Government retains nonexclusive, royalty-free license to publish or reproduce the published form of this contribution, or to allow others to do so, for U.S. Government purposes. Los Alamos National Laboratory requests that the publisher identify this article as work performed under the auspices of the U.S. Department of Energy. Los Alamos National Laboratory strongly supports academic freedom and a researcher's right to publish; as an institution, however, the Laboratory does not endorse the viewpoint of a publication or guarantee its technical correctness.

In-Situ DIC and Strain Gauges to Isolate the Deficiencies in a Model for Indentation Including Anisotropic Plasticity

Jacob S. Merson, Michael B. Prime, Manuel L. Lovato, Cheng Liu
Los Alamos National Laboratory, P.O. Box 1663, Los Alamos, NM 87545

ABSTRACT

A 60-mm diameter disk of 2024 aluminum was indented by opposing steel indenters over a central 10 mm region. Residual stress measurements made using neutron diffraction and the contour method matched each other, but not a finite element (FE) model with a calibrated model for plastic anisotropy of the aluminum. Since residual stresses are only the endpoint of the process, *in situ* data was needed to determine which portion of the load/unload process was causing model deficiencies. The indentation process was repeated on a new specimen with three-dimensional Digital Image Correlation (3D-DIC) to map full-field strain information and with resistance strain gauges to obtain high fidelity strain information at discrete locations. The DIC data was too noisy to extract strains, so displacements were analyzed after rigid body motion was removed. The deformation field revealed geometric imperfections of the indenters that were within tolerance, but had significant effect on the stress state. An updated FE model including geometric imperfections in the indenters gave better agreement with the DIC data. It did not however allow the material model to become the dominant effect and thus model calibration was unsuccessful.

Keywords: residual stress, digital image correlation, plastic anisotropy, finite element model, strain gauges

INTRODUCTION

Residual stresses play a significant role in many material failure processes like fatigue, fracture, fretting fatigue, and stress corrosion cracking [1-3]. Residual stresses are the stresses present in a part free from external load, and they are generated by virtually any manufacturing process. Because of their important contribution to failure and their almost universal presence, knowledge of residual stress is crucial for prediction of the life of any engineering structure. However, the prediction of residual stresses is a very complex problem. In fact, the development of residual stress generally involves nonlinear material behavior, phase transformation, coupled mechanical and thermal problems and also heterogeneous mechanical properties [4-15].

This paper discusses *in situ* data collection to improve a process model used to predict residual stresses. It shows how the use of different measurement techniques and multiple channels of data can help improve problem understanding.

BACKSTORY

To provide specimens for development and validation of techniques for residual stress measurement, solid disks were indented plastically by opposing, hardened-steel indenters, see Figure 1, a process occasionally used to introduce residual stresses for testing purposes [16]. A first set of specimens had 316L stainless steel as the disk material and the residual stresses were measured using neutron diffraction and the contour method [17,18]. An early finite element (FE) model, which used a calibrated stress-strain curve but assumed isotropic hardening, did not match the measurements very well [19]. Further testing of the 316L steel revealed a modest Bauschinger effect in cyclic stress-strain data. After calibrating a combined hardening model to the cyclic data, the FE model was able to match the measured stresses quite well [17].

Additional specimens were later made with the same indentation process but using 60-mm diameter, 10-mm thick disks of 2024-T351 Aluminum [20]. Based on the experience with 316L steel, a combined hardening model was calibrated on cyclic data, but the resulting FE model did not agree very well with measured residual stresses and strains. Further testing revealed that the 2024 Aluminum was mildly plastically anisotropic, see Figure 2, with lower strength in the in-plane direction transverse to the rolling direction of the original plate material, and higher but equal strength in the other two directions. An anisotropic plasticity model was calibrated to the data in Figure 2 and used to model the indentation. Figure 3 shows that neutron diffraction measurements were made along orthogonal paths along the rolling and transverse directions in the disk. Figure 4 shows residual hoop stresses along those two measurement scans (note that unplotted contour method [21] and slitting method [22] measurements validate the neutron results [20,19]). Switching to the anisotropic plasticity model significantly improved the model prediction, which now matches the difference in the residual stresses along the two measurement directions, but the predictions are still off of the data by about 50 MPa.

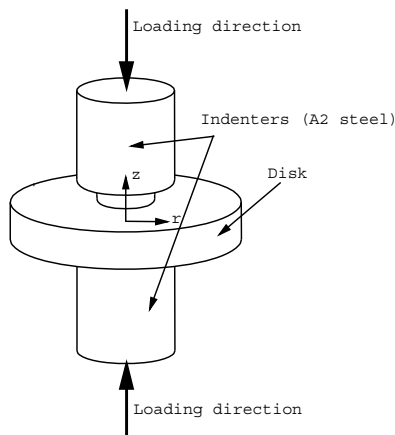


Figure 1 Indented disk residual stress specimens were made using 2024-T351 Aluminum disks

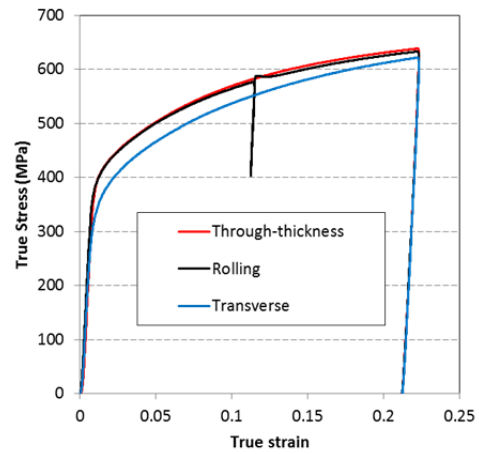


Figure 2 Mild plastic anisotropy in stress-strain curves for 2024 Aluminum.

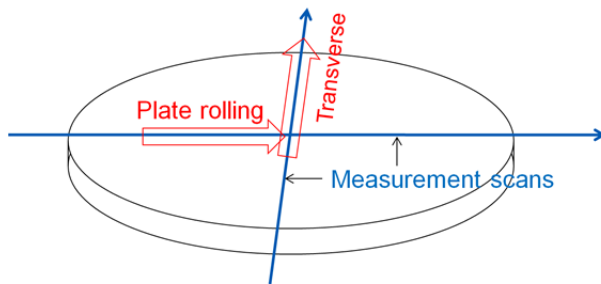


Figure 3 Neutron diffraction scans were made along two orthogonal directions

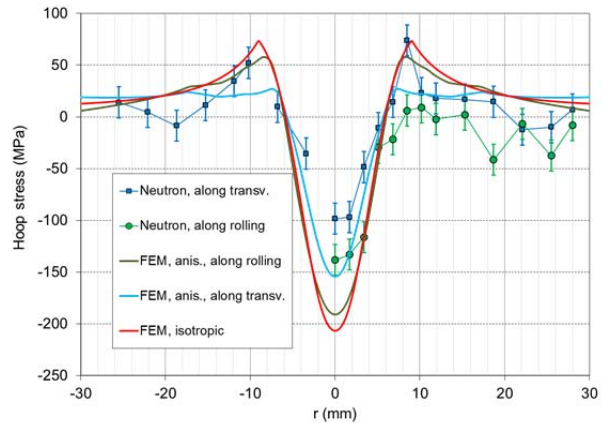


Figure 4 Even the anisotropic plasticity model does not agree well with the neutron measurements.

Purpose

The work in this paper aims to improve the FE model prediction shown in Figure 4. Several possible issues with the model have been discounted based on previous work:

- The anisotropic constitutive model already matches uniaxial compression data in all three material directions.
- Computational studies have demonstrated that the Bauschinger effect in 2024 Aluminum, measured in uniaxial cyclic testing, does not seem to have any effect on the prediction.¹
- Since there is significant hydrostatic compression under the indenter, a model for pressure-dependent plasticity in 2024 Aluminum [23] was implemented, and also shown to not significantly improve the model prediction [24].

The current data on these disks, mostly residual stresses and strains, only give information about the end state of the indentation process. End state data is insufficient to identify when during the process the model is deficient. The approach in this work, therefore, is to identify the deficiencies in the model by taking *in situ* data throughout the loading and unloading process of indentation in order to hopefully identify where the model has gone wrong and then fix it.

Methods

Experimental

The opposed indentation test sketched in Figure 1 was conducted with a 2024-T351 aluminum disk in an MTS 1125 load frame. The overall setup is shown in Figure 5. The indenters were coated in Molicote lubricant to reduce friction. Two PMMA rings were used to center the indenters on the disk. To accommodate DIC measurements, the top centering ring was removed before loading the sample. The crosshead was moved at 0.14 mm/min to reach a maximum load of 99.5 kN in about 10 minutes. Once maximum loading was achieved, the crosshead was reversed until the disk was completely unloaded.

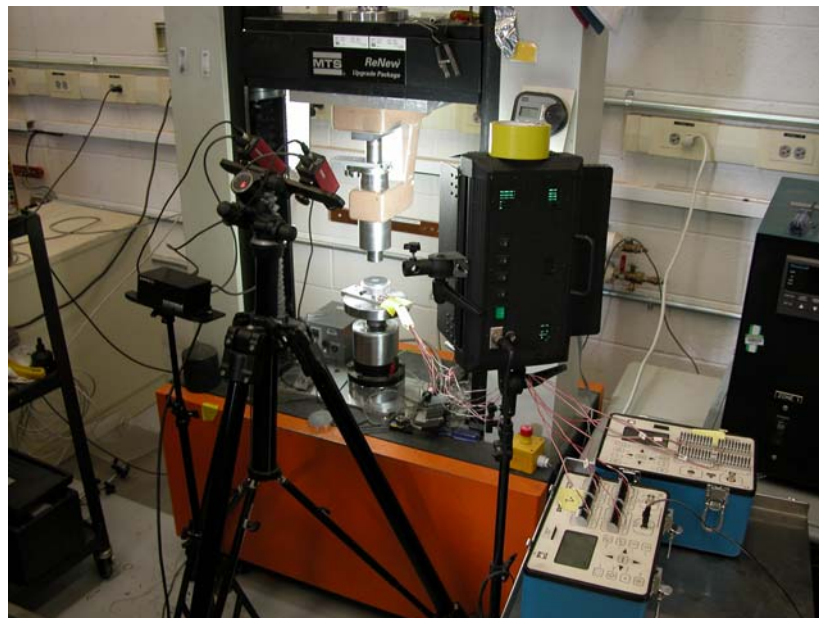


Figure 5 Experimental setup prior to inserting the top indenter.

¹ Fortunate, because modeling combined hardening simultaneously with anisotropic plasticity is quite limited using only the built-in functionality in the Abaqus commercial finite element code.

Strain gauges were used on one face of the disk, and the locations of strain gauges were optimized to be most sensitive to material modeling. A finite element model was run with several variations on the anisotropic material model for Al 2024. The predicted strain output at many locations was compared for the various material models to see where the differences were most significant. Based on the simulations, strain gauges were placed at 5 discrete locations shown in Figure 6. Three locations used stacked gauges to measure both hoop and radial strain and the two other locations measured radial strain, for 8 total channels of strain. Most of the gauges were along either the plate rolling or transverse directions, with some 10 mm from the center and others at 15mm, and one gauge was at 45 degrees to these axes in accordance with [25]. Strain was recorded at a sampling frequency of 1Hz. The 8 strain gauges were calibrated, and the data was collected with two Vishay model P3 Strain Indicator and Recorders.

In order to get a full field deformation map an optical technique called three-dimensional digital image correlation (3D-DIC) was used. DIC uses a computer vision approach to get a deformation field by comparing a set of before and after pictures. To capture the *in situ* strain field a series of images are taken and compared to the initial image. In order to capture out of plane motion a stereoscopic two camera system is used. A more detailed description of the DIC technique can be found in literature e.g. [26]. To measure the strain field the internal camera parameters must be calibrated. These parameters include the focal length, image center, distortions, skew, etc. Also, the relative positions and orientations of the cameras must be known for triangulation. Calibration allows calculation of parameters such as accuracy, uncertainty, and sensitivity.

To use 3D-DIC a speckle pattern must be added onto the surface of the disk. Black spray paint was used to create the speckles directly on the aluminum surface, see Figure 7. The thickness of these speckles is on the order of 1 micron. Since the black highly contrasted with the aluminum color, no background painting was necessary. In this experiment, the central 15mm and far half of the aluminum disk are hidden from view by the indenter and load frame during the indentation. However, pictures taken before and after the test allowed the final deformation to be determined over the full 360° disk surface minus the central 15 mm where the indenter had contacted the disk. During the indentation process DIC images were recorded at a frequency of 0.5 Hz.

Quantitative investigations regarding the confidence margins and errors in experimental measurements using DIC, both 2D and 3D, have been carried out in recent years [27-29]. One detailed investigation found a resolution in determining the in-plane motion within 0.006 pixels and the resulting variability for in-plane strain in the range of 20–90 $\mu\epsilon$ [28]. However, there are many factors that will affect the resolution and accuracy of DIC measurement, and the more significant uncertainty comes from the calibration of the 3D-DIC system. In our particular system, the calibration process indicates the uncertainty is less than 0.05 pixels. With spatial resolution of 45.5 $\mu\text{m}/\text{pixel}$, we expect the uncertainty in the in-plane displacement measurement to be about 2.3 μm and out-of-plane displacement measurement to be about 4.5 μm , which is twice of that in-plane uncertainty [27]. Scaling up from the reported results for 0.006 pixel resolution [28] to our value of 0.05 pixels, we estimate strain variability in the range 170–750 $\mu\epsilon$.

LED lights are used to provide sufficient light on the testing specimen for DIC measurements. The load cell and the DIC cameras use a synchronized clock and the clock on the strain gauge data is matched using a manual timing synchronization (e.g. strain gauges started at $t = 0\text{s}$, loading starts at $t = 30\text{s}$) and this is confirmed by matching the time of peak loading.

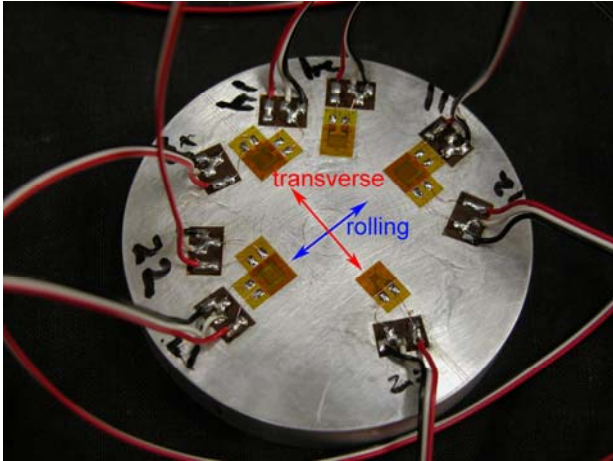


Figure 6 A total of 8 resistance strain gauges were used to measure hoop and radial strain in multiple directions.



Figure 7 The disk specimen shown during the indentation test. The DIC speckle pattern is visible on the top face of the disk.

Due to the relatively low deformations because of the highly constrained nature of the loading conditions, the strains measured with DIC were very noisy and were not very informative, see Figure 8. Therefore, displacements were used for comparing with the finite element model. To compare displacements, rigid body motion in the DIC of the part was calculated using a least squares fit of Q and b in equation (1).

$$Y = Q \cdot X + b \quad (1)$$

Where Y is the position vector (e.g. $Y = (x + u, y + v, z + w)$), Q is a third order orthogonal (rotation) tensor, X is the original position of each point, and b is the translation vector. From the DIC outputs, Y and X are known. Therefore, the displacement with no rigid body motion U can be written as equation (2).

$$U = Y - (Q \cdot x + b) \quad (2)$$

These rigid body motions were subtracted from the deformation field, and a transformation into a cylindrical coordinate system was done for visual inspection of the deformation field. This inspection gave a good comparison of the deformation field to the finite element model.

Considering that the loading was nominally axisymmetric but that the aluminum was anisotropic as shown in Figure 2, the deformation field was expected to be different in the rolling and transverse directions but symmetric about those two axes. Instead the deformation was asymmetric, as is shown later in Figure 12, with the transverse-direction deformations notably greater on one side of the indenter than the other. This asymmetry indicated that the loading was not as axisymmetric as intended.

In order to investigate and quantify this asymmetry the indenters and disk indentations were inspected using a coordinate measuring machine (CMM). Figure 9 shows the results for the bottom surface of the disk. Using least squares fit of a plane on the bottom of the indent, a tilt of 0.064 degrees was estimated, which translates to about 15 microns of tilt over a 15mm diameter, or about 60% of the average indent depth. This is within the specified machining tolerances of the indenters, but is significant relative to the assumption of axisymmetric loading. The indent on the top surface of the disk, the surface measured by DIC in Figure 7, was tilted by about 0.019 degrees relative to the surface of the disk, corresponding to about 5 microns of tilt or 20% of the indent depth. On both the top and bottom surfaces, the low point of the indentation aligned with neither the rolling or transverse axis but was rather between the two. Inspection of the two indenters revealed that the indentation surfaces were tilted 0.033 and 0.008 degrees relative to the opposite surface if the indenter, but the precision of the alignment of the platens on the load

frame is not known, so it is not clear what angle the indenter actually makes with the disk surface. Indenter tilt turns out to be an important factor which must be accounted for in the finite element models.

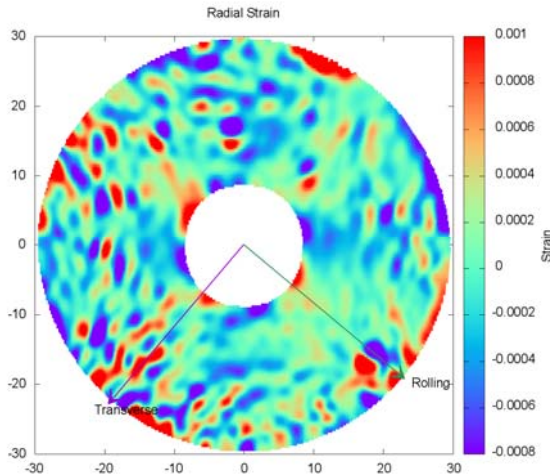


Figure 8. A plot of radial strain from the DIC shows that the strain is low and, therefore, too noisy to be helpful

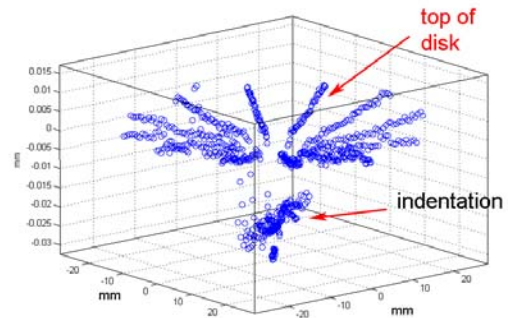


Figure 9 CMM inspection data on the bottom of the indented disk. The data is plotted such that the top of the surface is approximately flat at a height of 0. The bottom of the indent is tilted

Finite Element Modeling

The disk indentation process was modeled as a quasi-static process in Abaqus/Standard finite element code. All models were assumed to have nonlinear geometries. In previous work, the model progressed from a 2-D axisymmetric model [19], which could only look at isotropic material behavior, to a 1/8th symmetry 3D finite element model in order to model material anisotropy. Based on DIC and inspection results (e.g., Figure 9), a 1/8th symmetry model was no longer adequate so a full 3D model which accounted for indenter tilt and in-plane angle (where the low point of the indenter was aligned) was created. Table 1 shows the number of 20 noded reduced integration elements (C3D30R) used in the rough and fine meshes. The rough mesh, shown in Figure 10, was used for most of the calculations in this paper as the difference in the strain and contour outputs was negligible. The mesh in the contact zone was selected to be fine enough to help reduce local perturbations at the edge of the contact region.

Table 1 Number of elements in rough and fine meshes used in finite element calculations

Part	Elements in Rough Mesh	Elements in Fine Mesh
Top Indenter	384	4032
Bottom Indenter	384	3976
Disk	7794	70686
Total	8562	78694

Determining the boundary conditions for problem was challenging. A displacement condition was used to apply the load on the indenters, and the displacement value was adjusted so the total load matched the experiment (99.5kN). The indenter had rotation about its own axis constrained as we assume the friction

between the platen and indenter is strong enough to oppose rotation. The disk was constrained so it couldn't rotate out of plane because unconstrained models predicted such a rotation (Figure 11) and failed to match observed indentation patterns. We believe that the PMMA fixture used to align the indenter and disks provided sufficient constraint to prevent such rotation.

Correctly modeling the contact also presented a challenge. Abaqus surface to surface contact was used with a stabilization factor of one, and end of step stabilization factor of 0.1. These stabilization values were chosen to maximize solution speed while keeping the associated dissipative energies below 1% of the total system energy.

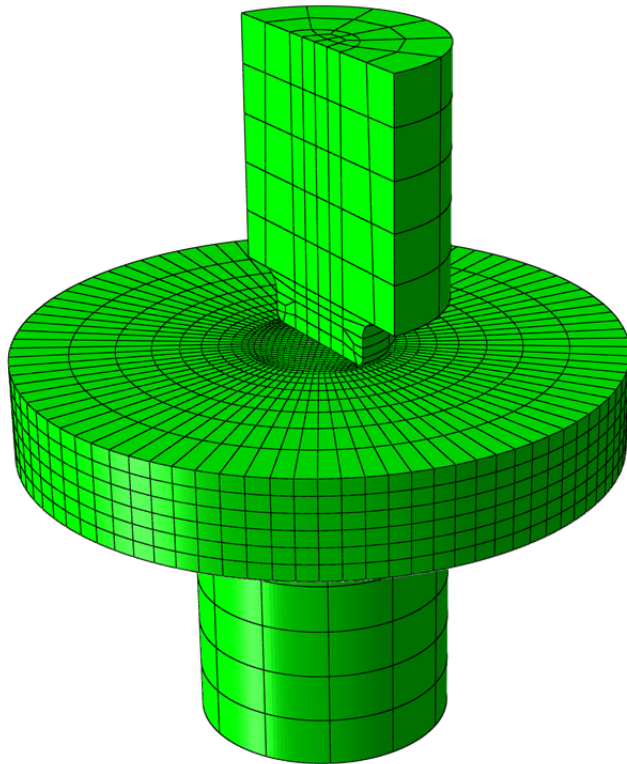


Figure 10. The mesh for the indentation process model is most refined in the indentation region where the largest gradients occur. In this graphic, half of the upper indenter is removed to expose the underlying mesh.

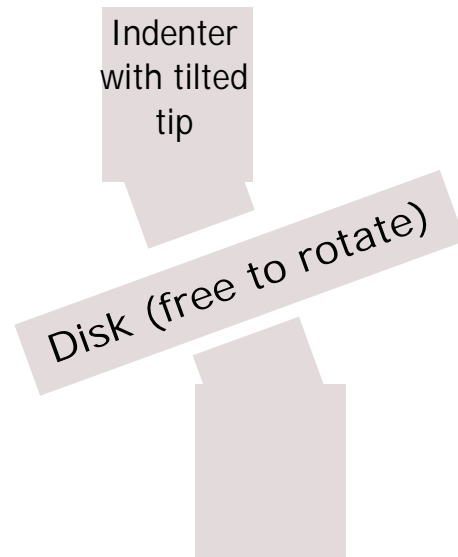


Figure 11 Unconstrained models allowed a disk rotation that was not observed experimentally. Hence, constraints were added to the model.

Material Models

The material modeling was similar to previous efforts to model this indentation process [24]. The indenter material used was A2 tool steel characterized by a high hardness (58 HRC) and a high yield stress (about 1300 MPa), so the indenter was modeled as elastic with Young's modulus of 204 GPa and Poisson's ratio of 0.3. For the Al 2024, the Young's modulus was 73.2 GPa and Poisson's ratio was 0.33. As discussed previously, an anisotropic plasticity model using isotropic hardening (no Bauschinger effect) was used. Plastic anisotropy was modeled using Hill's potential function [25] in ABAQUS. Because the conversion of uniaxial stress-strain curves to effective-stress – effective-strain curves depends on the R ratios, the ratios between the strengths in different directions, an iterative process was used to fit the R ratios to the data [24]. This fit was applied in ABAQUS using the *POTENTIAL function to define the anisotropy and a tabular description of the stress-strain curve.

Results and Discussion

The finite element model was able to reasonably reproduce the tilt in the bottom of the indentation (e.g., Figure 9) measured by the CMM. The model predicted a tilt of 0.055 degrees on the bottom indent compared to the measured value of 0.064 degrees, and the predicted tilt on the top surface was 0.022 degrees compared to the measured value of 0.019 degrees, so both within 16% of experiment. Because the alignment of the platens in the load frame is uncertain, it would be reasonable to iterate on the initial indenter tilt until even better agreement was achieved. However, the current level of agreement is sufficient to evaluate the effects on indenter tilt on predictions of deformation and strain.

Figure 12 shows the radial deformation field at the end of the indentation and unloading process measured by 3D-DIC, after removal of rigid body motions. Visually inspecting the deformation field shows that the areas of maximum radial deformation are asymmetric, being greater on one side (upper right quadrant of Figure 12) than the opposite side. This key observation led to the inescapable conclusion that the load was asymmetric, which led to geometry quantification using CMM measurements, and then model refinement. Figure 13 shows that the finite element model including indenter tilt predicts a similar asymmetry in the deformation field.

It was challenging to get useable DIC data since the strains resulting from indentation were very small. Practical use of DIC data required analysis of the deformations and thus removal of the rigid body motion. The process used to remove rigid body motion from the before and after picture with full disk visibility did not work on the *in situ* measurements when only half of the disk was visible. For the *in situ* deformation field, further work must be done to remove the rigid body motions so that the results can be compared with FEM.

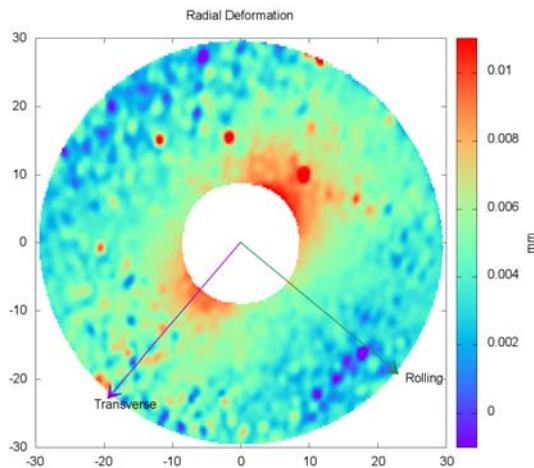


Figure 12 Radial deformation field from DIC results. Note that the asymmetry around the indent helped to diagnose the tilt in the indenter.

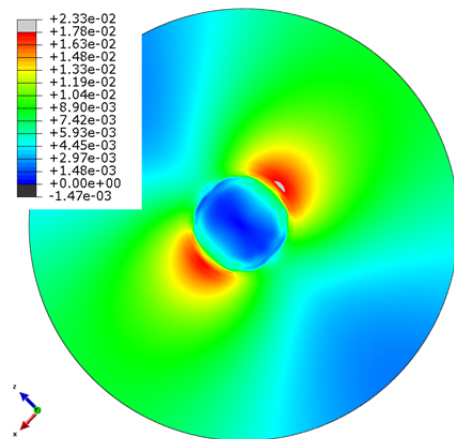


Figure 13 Contour Plot of radial deformation (in mm) from finite element model. Here the transverse axis is pointing down. Note asymmetry in the deformation field around the indentation.

We now present comparisons of the FE model to representative strain gauge data. The title of each plot identifies which strain gauge from Figure 6 is shown using three identifiers in order at the end of the plot title:

- The radial distance from the center of the disk to the strain gauge center, either 10 or 15 mm
- The *location* of the gauge, either rolling axis (along the blue line in Figure 6), transverse (red line in Figure 6) or 45 degrees.

- The component of strain being measured, either hoop or radial.

The comparisons will also show two variations on the anisotropic plasticity model. “Anisotropic plasticity 1” was an earlier rough version of the model, with slightly greater strength and anisotropy than version 2, which better matched the calibration data. For the case of anisotropic model 2, predictions are presented with and without indenter tilt. For an isotropic plasticity model, and anisotropic model 1, results are only presented for a flat (untilted) indenter.

To aid interpretation of the strain plots, one should first understand the basic deformation modes [17]. During indentation, the material under the indenter is compressed thinner and therefore wants to expand radially. The material radially outside the indenter (where the strain gauges are) then deforms like a ring under internal pressure: compression in the radial direction and tension in the hoop direction.

Figure 14 and Figure 15 show the only load-strain curves where adding the indenter tilt made a notable improvement to the prediction, and even there the improvement is debatable. These are the two radial strain measurements closer to the indenter ($r = 10$ mm), and they show an unusual shape. Unlike all the other curves, these two have a change in the sign of the slope during loading, and unlike we just described in the previous paragraph, these radial strain start out positive. Near but outside the indenter region, the surface material of the disk is pulled axially towards the disk mid thickness, which stretches that material into tension. Later, the aforementioned radial expansion of the material under the indenter begins to dominate and turn the strains towards compression. Adding the indenter tilt has improved the model prediction near the peak load, although in the case of Figure 14, all of the models do a poor job of predicting the data.

Both of those figures, along with Figure 16 and others show that adding the indenter tilt predicts a significant nonlinear transient at early loads. The data generally shows linear elastic behavior, especially all the data taken at $r = 15$ mm. At this time, the reason for the discrepancy is not fully understood, but it is striking. It appears to be a geometric nonlinearity before there is any yielding, and may have something to do with the contact numerics.

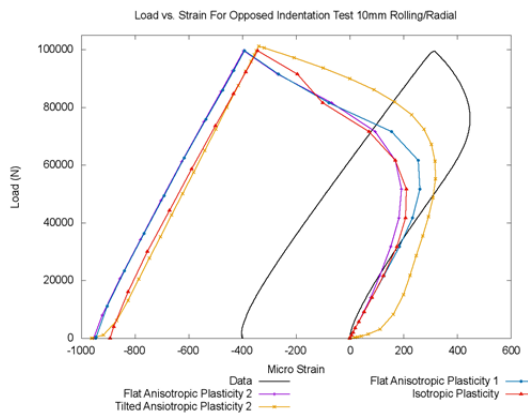


Figure 14 Load vs strain curve at 10 mm on the rolling axis in the radial direction.

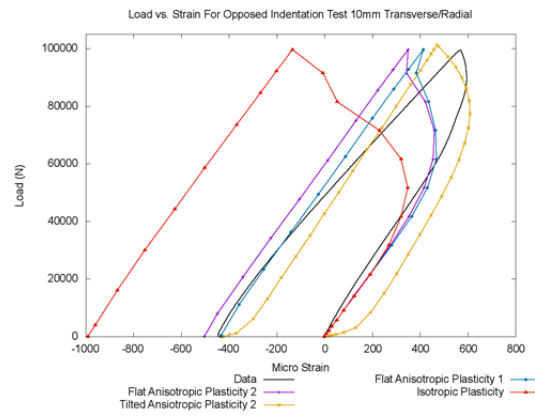


Figure 15 Load vs strain curve at 10 mm on the transverse axis in the radial direction.

The tilted-indenter model also did not significantly change the residual stress prediction of Figure 4, which was the main purpose of this effort. Therefore, the effort to model the indenter tilt and related geometric issues may have been an unproductive effort – a red herring. Adding indenter tilt did improve comparison with two sets of data: the DIC deformations and the CMM-measured shapes of the indentations. Adding

the tilt generally made the strain predictions worse. Adding the tilt did not change the most important comparison with data: the residual stresses. Overall, the tilted indenter model gave a very mixed result with better agreement on only two out of four measures.

Figure 15 and Figure 16 show that changing from an isotropic plasticity model to either of the anisotropic models has significantly improved the prediction, which is encouraging. In a few cases, like Figure 14, there is no noticeable improvement from an anisotropic model although it is also no worse.

Some of the strain data is also quite sensitive to the variations in the material model. To see this compare the untilted (flat) predictions of the two anisotropic models. In some cases, like Figure 17 and Figure 18, anisotropic model 1, gives a noticeably superior prediction. In other cases, like Figure 16, model 2 is superior and in others, like Figure 19, none of the models predict the data well.

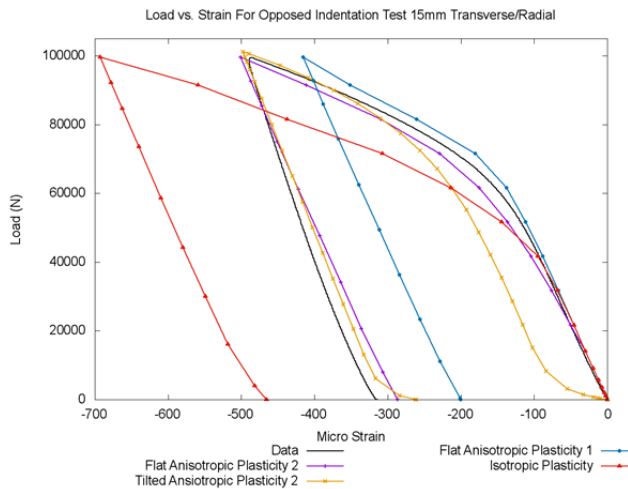


Figure 16 Load vs strain curve at 15 mm on the transverse axis in the radial direction.

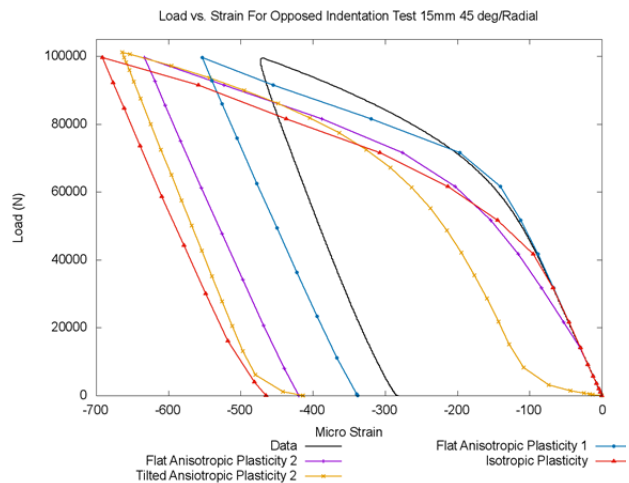


Figure 17 Load vs strain curve at 15 mm on the 45° axis in the radial direction.

The inability of the titled indenter model to match more of the data was disappointing and led to further investigation. The previous CMM data had been collected independently on each face of the disk. More CMM data was collected but on both faces simultaneously. It was determined that the disk faces were tilted 0.024 degrees in relation to each other, which is significant relative to the indentation tilts measured relative to each face (0.064 and 0.019 degrees). These face tilts could have a significant impact on the measured strain field because it will affect the loading alignment with the tilted indenters. However, we do not expect that changing only that issue in the models would results in a wholesale improvement of the prediction.

In this indentation process the hydrostatic loading conditions (stiff indenter on a stiff disk with deformation constrained in all three directions under the indenter) lead to high sensitivity to small geometric changes. The strain gauges are able to capture these changes with high sensitivity. The full-field DIC data is able to capture global physics; however in comparison to the strain gauges it has limited sensitivity.

One important aspect of this work is the use of multiple types and locations of data to create a unique inverse problem. This is important because it allows confidence that when agreement is found all of the underlying physical phenomenon have been captured. In this case, we have not achieved satisfactory agreement.

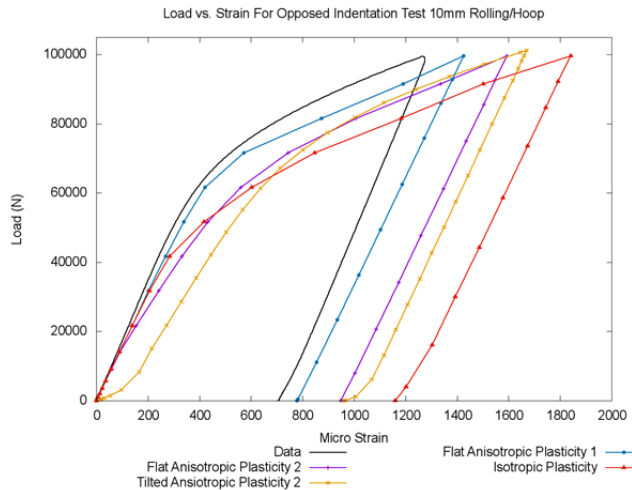


Figure 18 Load vs strain curve at 10 mm on the rolling axis in the hoop direction.

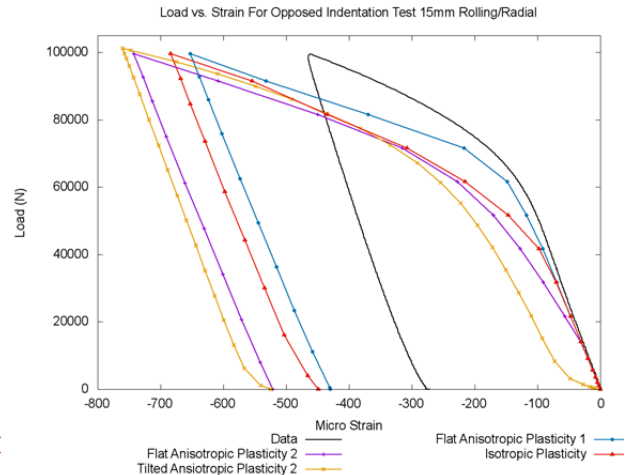


Figure 19 Load vs strain curve at 15 mm on the rolling axis in the radial direction.

Conclusions

In this paper the use of multimodal data allowed a much deeper understanding of the problem physics at hand:

- Only the *full field data* from 3D-DIC was able to identify the key geometric issues (tilting) in the indenters. This would not have been discovered through the strain gauge data alone.
- Only the strain gauges had sufficiently high precision to be sensitive to small changes in geometry and material model.
- Unfortunately, the unexpected sensitivity to small geometric perturbations made it too difficult to isolate material modeling effects and study those.

As seen above, the strain gauge data improved in some locations and got worse in others while the DIC deformation field was insensitive to these changes. This shows that if we had collected data at only one or two points, then we might have matched our experimental data without getting the correct solution. Using many sources of data to interpret model agreement allows us to be certain that we have created a unique inverse problem (reduced the likelihood of falsely matching data).

In the end, we were unable to isolate all errors in the model and improve the prediction of residual stresses.

If we could capture all the geometric details perfectly, we might be able to isolate the effects of the material model. One approach would be to repeat the test with better controls. We could use the inspection data from the indenters to make the orientation and magnitude of the indenter tilt a known quantity. Also, to make the boundary conditions on the disk more obvious, both the top and bottom centering rings could be removed during the experiment and additional displacement measurements could be taken to check boundary conditions. On the other hand, a specimen re-design could be even more helpful. In order to remove geometric issues with the indenter tilt an indenter with a curved surface could be used. However, with this highly stiff and constrained loading configuration, other alignment issues might still be significant.

ACKNOWLEDGEMENTS

This work was performed at Los Alamos National Laboratory, operated by the Los Alamos National Security, LLC for the National Nuclear Security Administration of the U.S. Department of Energy under

contract DE-AC52-06NA25396. By acceptance of this article, the publisher recognizes that the U.S. Government retains a nonexclusive, royalty-free license to publish or reproduce the published form of this contribution, or to allow others to do so, for U.S. Government purposes.

REFERENCES

1. Withers PJ (2007) Residual stress and its role in failure. *Reports on Progress in Physics* 70 (12):2211-2264
2. James MN (2011) Residual stress influences on structural reliability. *Engineering Failure Analysis* 18 (8):1909-1920
3. Liu KK, Hill MR (2009) The effects of laser peening and shot peening on fretting fatigue in Ti-6Al-4V coupons. *Tribology International* 42 (9):1250-1262
4. Edwards L, Smith MC, Turski M, Fitzpatrick ME, Bouchard PJ (2008) Advances in residual stress modeling and measurement for the structural integrity assessment of welded thermal power plant. *Advanced Materials Research* 41-42:391-400
5. Aydiner CC, Ustundag E, Prime MB, Peker A (2003) Modeling and measurement of residual stresses in a bulk metallic glass plate. *Journal of Non-Crystalline Solids* 316 (1):82-95
6. Tanner DA, Robinson JS (2003) Modelling stress reduction techniques of cold compression and stretching in wrought aluminium alloy products. *Finite Elements in Analysis and Design* 39 (5/6):369-386
7. Yaghi AH, Hilson G, Simandjuntak S, Flewitt PEJ, Pavier MJ, Smith DJ, Hyde TH, Becker AA, Sun W (2010) A Comparison Between Measured and Modeled Residual Stresses in a Circumferentially Butt-Welded P91 Steel Pipe. *Journal of Pressure Vessel Technology* 132 (1):011206-011206. doi:10.1115/1.4000347
8. Rolph J, Preuss M, Iqbal N, Hofmann M, Nikov S, Hardy MC, Glavicic MG, Ramanathan R, Evans A (2012) Residual Stress Evolution during Manufacture of Aerospace Forgings. Huron ES, Reed RC, Hardy MC et al. (eds) *Superalloys 2012*. John Wiley & Sons, Inc., Hoboken, NJ, USA, pp 881-891. doi:10.1002/9781118516430.ch97
9. Dai H, Francis JA, Withers PJ (2010) Prediction of residual stress distributions for single weld beads deposited on to SA508 steel including phase transformation effects. *Materials Science and Technology* 26:940-949. doi:10.1179/026708309x12459430509454
10. DeWald AT, Hill MR (2009) Eigenstrain based model for prediction of laser peening residual stresses in arbitrary 3D bodies. Part 1: model description. *Journal of Strain Analysis for Engineering Design* 44 (1):1-11
11. Prime MB, Prantil VC, Rangaswamy P, Garcia FP (2000) Residual stress measurement and prediction in a hardened steel ring. *Materials Science Forum* 347-349:223-228
12. Muránsky O, Hamelin CJ, Smith MC, Bendeich PJ, Edwards L (2014) The Role of Plasticity Theory on the Predicted Residual Stress Field of Weld Structures. *Materials Science Forum* 772:65-71
13. Carlone P, Palazzo GS, Pasquino R (2010) Finite element analysis of the steel quenching process: Temperature field and solid–solid phase change. *Computers & Mathematics with Applications* 59 (1):585-594. doi:<http://dx.doi.org/10.1016/j.camwa.2009.06.006>
14. Tanner DA, Robinson JS (2000) Residual stress prediction and determination in 7010 aluminum alloy forgings. *Experimental Mechanics* 40 (1):75-82. doi:10.1007/bf02327551
15. Ismonov S, Daniewicz SR, Newman JJC, Hill MR, Urban MR (2009) Three Dimensional Finite Element Analysis of a Split-Sleeve Cold Expansion Process. *Journal of Engineering Materials and Technology* 131 (3):031007. doi:10.1115/1.3120392
16. Mahmoudi AH, Stefanescu D, Hossain S, Truman CE, Smith DJ, Withers PJ (2006) Measurement and prediction of the residual stress field generated by side-punching. *Journal of Engineering Materials and Technology* 128:451-459
17. Pagliaro P, Prime MB, Clausen B, Lovato ML, Zuccarello B (2009) Known Residual Stress Specimens Using Opposed Indentation. *Journal of Engineering Materials and Technology* 131:031002
18. Pagliaro P, Prime MB, Swenson H, Zuccarello B (2010) Measuring Multiple Residual-Stress Components Using the Contour Method and Multiple Cuts. *Experimental Mechanics* 50 (2):187-194. doi:10.1007/s11340-009-9280-3
19. Pagliaro P (2008) Mapping Multiple Residual Stress Components Using the Contour Method and Superposition. Ph.D. Dissertation, Università degli Studi di Palermo, Palermo

20. Pagliaro P, Prime MB, Robinson JS, Clausen B, Swenson H, Steinzig M, Zuccarello B (2011) Measuring Inaccessible Residual Stresses Using Multiple Methods and Superposition. *Experimental Mechanics* 51 (7):1123-1134. doi:10.1007/s11340-010-9424-5
21. Prime MB, DeWald AT (2013) The Contour Method. Schajer GS (ed) *Practical Residual Stress Measurement Methods*. John Wiley & Sons, Ltd., Chichester, WestSussex, UK. doi:10.1002/9781118402832.ch5
22. Hill MR (2013) The Slitting Method. Schajer GS (ed) *Practical Residual Stress Measurement Methods*. John Wiley & Sons, Ltd, pp 89-108. doi:10.1002/9781118402832.ch4
23. Bai Y, Wierzbicki T (2008) A new model of metal plasticity and fracture with pressure and Lode dependence. *International Journal of Plasticity* 24 (6):1071-1096
24. Prime MB (2013) Anisotropic and Pressure-Dependent Plasticity Modeling for Residual Stress Prediction. Ventura CE, Crone WC, Furlong C (eds) *Experimental and Applied Mechanics, Volume 4, Conference Proceedings of the Society for Experimental Mechanics Series. Conference Proceedings of the Society for Experimental Mechanics Series*. Springer New York, pp 415-427. doi:10.1007/978-1-4614-4226-4_49
25. Hill R (1948) A Theory of the Yielding and Plastic Flow of Anisotropic Metals. *Proceedings of the Royal Society of London Series A Mathematical and Physical Sciences* 193 (1033):281-297. doi:10.1098/rspa.1948.0045
26. Sutton MA, McNeill SR, Helm JD, Chao YJ (2000) Advances in Two-Dimensional and Three-Dimensional Computer Vision. Rastogi P (ed) *Photomechanics*, vol 77. Topics in Applied Physics. Springer Berlin Heidelberg, pp 323-372. doi:10.1007/3-540-48800-6_10
27. Wang YQ, Sutton MA, Ke XD, Schreier HW, Reu PL, Miller TJ (2011) On Error Assessment in Stereo-based Deformation Measurements. *Experimental Mechanics* 51 (4):405-422. doi:10.1007/s11340-010-9449-9
28. Ke XD, Schreier HW, Sutton MA, Wang YQ (2011) Error Assessment in Stereo-based Deformation Measurements. *Experimental Mechanics* 51 (4):423-441. doi:10.1007/s11340-010-9450-3
29. Reu PL (2011) Experimental and Numerical Methods for Exact Subpixel Shifting. *Experimental Mechanics* 51 (4):443-452. doi:10.1007/s11340-010-9417-4